

# GRAIN-BOUNDARY OXIDATION OF USED CANDU FUEL EXPOSED TO DRY AIR AT 150°C FOR A PROLONGED PERIOD

W.H. HOCKING, R. BEHNKE, A.M. DUCLOS, A.F. GERWING AND K.M. WASYWICH

Atomic Energy of Canada Limited  
Whiteshell Laboratories  
Pinawa, Manitoba, Canada R0E 1L0

## ABSTRACT

The grain-boundary chemistry of used CANDU fuel exposed to dry air at 150°C for a prolonged period has been investigated by X-ray photoelectron spectroscopy (XPS) and scanning electron microscopy (SEM). High degrees of surface oxidation have been determined using the chemical-shift effect for the uranium photoelectron emission, but these must be largely restricted to thin films. The observed distribution of segregated fission products implies an absence of major fuel restructuring and SEM examinations revealed mainly subtle changes in the  $\text{UO}_2$  grain structure. These findings are consistent with metallographic evidence of pervasive grain-boundary attack, despite only slight bulk alteration of the fluorite-lattice structure.

## 1. INTRODUCTION

The used fuel discharged from nuclear power reactors is traditionally stored in water pools to dissipate the decay heat. Long-term fuel storage in concrete canisters, following an initial pool-cooling period of ~10 years, has become increasingly attractive [1-3]. Dry storage of used CANDU fuel has been demonstrated in Canada and similar programs are planned or underway in several other countries. An extended study of the potential for progressive degradation of used CANDU fuel during such storage was undertaken in 1980 [2-5]. Intact and intentionally defected fuel elements, spanning a wide range of fabrication parameters and power histories, were stored at 150°C in sealed containers filled with either dry air or moisture-saturated air — designated as CEX-1 and CEX-2 respectively (for Controlled Environment Experiment, Phase 1 and Phase 2). Destructive analysis of several defected elements from each of these experiments over the first decade of exposure revealed significant differences in the fuel oxidation behaviour [3]. Visible alteration of the fuel was largely restricted to the immediate vicinity of the defect in dry air, whereas grain-boundary oxidation was identified throughout the element in moist air. Because pronounced depletion of  $\text{O}_2$  from the storage-container atmosphere was also found in both cases, the experimental configuration was changed to provide either unlimited (but constricted) air access (CEX-1) or frequent air replenishment (CEX-2), which should more closely simulate the high air to exposed-fuel ratio expected under actual storage conditions.

Destructive analysis of four defected fuel elements after ~40 months in unlimited dry air at 150°C, with a cumulative exposure of ~140 months, has recently been completed. Extensive

grain pullout was observed in metallographically prepared sections along the full length of each element and indicates pervasive grain-boundary attack. Thorough characterization of the nature of that attack, by surface analysis of fuel fragments using scanning electron microscopy (SEM) and X-ray photoelectron spectroscopy (XPS), is summarized in this paper. The fracture mode, grain morphology and any secondary crystallization were revealed by the SEM examinations. Grain-boundary chemistry was investigated with high surface specificity by XPS, providing information not only on the uranium oxidation state but also on fission-product segregation and redistribution. Other aspects of the bulk properties of these exposed fuels are reported in a companion paper [6].

## 2. EXPERIMENTAL PROCEDURES

The used CANDU fuel elements that were destructively analyzed in the present study are identified in Table 1: the reactor of origin, Bruce (B) or Pickering (P), has been specified by the first letter in the bundle serial code, which is followed by the element number. Before the initial storage emplacement, each element had been intentionally defected by drilling a single 3 mm diameter hole through the Zircaloy sheath. Discrete fragments of fuel, ~3 mm in size, were extracted from element segments using minimum force to preferentially access well exposed cracks and grain-boundary interfaces. Vibrations during handling and sheath removal (cut open using an argon-cooled silicon carbide saw) were sufficient to cause extensive fragmentation of the weakened fuel pellets. The fragments were affixed to individual aluminum mounts with conductive, silver-based epoxy for XPS/SEM analysis. All of the preliminary operations were conducted remotely in a hot cell, because of the radiation fields involved; however, the final critical steps were performed manually, using long tweezers, in a shielded fumehood. Duplicate samples were taken from four different segments of each element, as specified in Table 1.

X-ray photoelectron spectra were recorded using a modified McPherson ESCA-36 instrument that has been specifically adapted for studies of small highly radioactive samples. Photoelectron emission was excited by Mg K $\alpha$  X-radiation and collected from an area of ~400  $\mu\text{m}$  by ~2 mm centred on the fragment. Further details of the procedures for instrument operation and data processing have been reported elsewhere [7-9]. Composition depth profiles were compiled by sequential XPS analysis and argon-ion sputtering, at a rate of 0.1 nm/min, calibrated using ion-implanted UO<sub>2</sub> standards [10]. After completion of the XPS studies, each fragment was sputter coated with a thin film of gold to prevent surface charging during the subsequent SEM examination. This was performed using a shielded Hitachi S-570 microscope equipped with a Microspec model 2A wavelength dispersive X-ray analyzer [11]. The fracture surface morphology can provide important confirmation or qualification of the suitability of a fragment for XPS analysis [8,9] — the results from only two samples (BF06605C/14 13-I and BE04323C/8 8-0 in Table 1) were completely rejected on that basis in the present study.

### 3. RESULTS AND DISCUSSION

#### 3.1 Grain-Boundary Oxidation

The degree of surface oxidation of each fuel fragment was determined from chemical-shift effects in the uranium photoelectron emission spectra. Curve-resolution of the broadened U 4f<sub>7/2</sub> peak envelope into two components yields a quantitative estimate of the proportions of uranium in the +4 and +6 valence states [3-5,9,12]. An independent check on the curve-resolved measurement is provided by the relative intensity of the U 5f peak, which progressively declines as UO<sub>2</sub> is oxidized to UO<sub>3</sub> (illustrated in Figure 1). The results for all fragments, expressed as %U<sup>6+</sup> and U<sup>6+</sup>/U<sup>4+</sup> ratio, are collected in Table 1. These data represent the extent of surface oxidation averaged over the escape depth of the photoelectrons (~2 nm) and the analysis area on the sample. An appraisal of the probable error range for the %U<sup>6+</sup> values has also been given, based on consideration of the statistical uncertainty, robustness of the fit and confidence in the surface-charging correction [3].

The measurements in Table 1 show no apparent correlation between radial location and the degree of surface oxidation of the fuel fragment, consistent with previous XPS studies of used CANDU fuels exposed to CEX-1 or CEX-2 conditions [3-5]. A large increase in the average %U<sup>6+</sup> has been found here (70 %U<sup>6+</sup> on average) in comparison with fuels exposed to limited air, in particular BF06605C/8 (43 %U<sup>6+</sup> on average after ~100 months in dry air at 150°C) [3]. This indicates that the unlimited air available during the last storage period has caused a significant advance in the extent of grain-boundary oxidation. Further consideration of the data in Table 1 reveals a lack of dependence on fuel power history but a weak trend with distance from the sheath defect — the highest %U<sup>6+</sup> values are always found near the defect. A different pattern has been observed for fuels exposed to CEX-2 conditions, where grain-boundary oxidation increases with the fuel power but is essentially uniform along the element length [3-5].

#### 3.2 Fragment Surface Morphology

A representative selection of secondary electron images depicting the surface morphology of the CEX-1 fuel fragments has been reproduced in Figures 2-5. The range of features observed reflects the power history of the fuels as well as the subsequent storage exposure and sampling methodology. Visible indications of surface alteration were surprisingly muted considering the other evidence of grain-boundary attack; specific observations on each fragment have been summarized in Table 1. The predominant overall trait was clean intergranular fracture, accented by grain-edge rounding and separation. A small contraction of the fluorite lattice that occurs when UO<sub>2</sub> is oxidized to U<sub>4</sub>O<sub>9</sub> or U<sub>3</sub>O<sub>7</sub> would be consistent with the latter [5,13]. About a third of all fragments exhibited at least one crack; however, it is uncertain whether these are entirely a manifestation of the fuel oxidation. Visible cracking of individual fuel grains was uncommon and possibly caused by physical damage (Figure 4d) incurred during fuel handling or sample selection. Some transgranular fracturing was also seen, but more typically appeared to reflect old, in-reactor cracks rather than fresh grain cleavage (Figures 2c, 2d and 4a).

The effects of reactor irradiation were still readily apparent on most of the fragment surfaces. Fission-gas bubbles and tunnels, decorated with  $\epsilon$ -phase (noble metal) particles [14], were identified on several fragments taken from near the centreline of the high-power fuels (Figures 3a, 4c and 4d). Extensive surface texture, which is characteristic of CANDU fuels [8,9], was observed on many other grain faces (Figures 3b, 3c, 4b and 5a). Secondary crystallization was probably found on a number of fragments as well, but in widely varying proportions and with different levels of certainty (Table 1). Sparse coverage by very fine-grained material, which may develop a cloud-like appearance, has been tentatively attributed to  $U_3O_8$  nucleation and growth (Figures 2c, 2d, 3d, 4a and 4b). Heavier deposits of less distinctive particulate may at least partly represent debris created by physical damage (Figures 5b, 5c and 5d).

### 3.3 Fission-Product Segregation

Pronounced segregation of certain fission products to cracks and grain boundaries in used CANDU fuels has now been well established through XPS studies of fragments taken from both intact elements and defected elements, after CEX-1 or CEX-2 exposure [4,8,9]. Chemical-shift measurements were indicative of oxidized species, probably mixed uranates. Segregation at monolayer-level coverages was demonstrated by sequential XPS analysis and argon-ion sputtering. Calculations based upon an idealized thin-film model were broadly consistent with the composition depth profiles and the known properties of CANDU fuels.

Representative low-binding-energy portions of XPS spectra recorded from typical fragments of the four CEX-1 fuels analyzed in the present study are compared in Figure 6. These show a marked dependence of fission-product segregation on fuel power history. The two high-power fuels both exhibit distinct Rb 3d and Ba 4d peaks as well as strong Cs 4d spin-orbit doublets; conversely, only weak Cs 4d emission has been detected from the two low-power fuels (more convincingly from BF06605C/14 than from BE04323C/8 in Figure 6, but the opposite for some other fragments from these two fuels). At the relatively low burnups achieved, CANLUB appears to have had little impact on fission-product segregation. Pre-storage fission-gas release (FGR) measurements and diametral  $\gamma$ -ray scans for cesium on other outer elements from the same bundles are sensibly correlated with the XPS results. The two high-power fuels had 4.5-7.2% FGR and up to 60% depletion of  $^{137}\text{Cs}$  from a central 5 mm core, whereas the two low-power fuels had <0.16% FGR and no radial  $^{137}\text{Cs}$  migration. A sequence of low-binding-energy XPS spectra collected from another fragment of P26244C/7 fuel, at increasing intervals of argon-ion sputtering, has been reproduced in Figure 7. The pattern of fission-product removal seen here is similar to that observed for fragments taken from intact elements and indicates monolayer-level surface coverage with probably some inhomogeneity [8].

Variability in the extent of fission-product segregation within the high-power fuels is illustrated in Figure 8; typically, the relative abundance of cesium differs less from one fragment to another than that of barium. A similar behaviour has been observed for intact fuels and can be pronounced also for tellurium, as shown by the representative selection of Te 3d spectra in Figure 9 that were collected from the high-power CEX-1 fuels. Because of the evident lack of correlation with location in the element, as seen in Figures 8 and 9, redistribution of fission products during the recent (and prior) CEX-1 storage would appear not to have been significant.

Air exposure at 150°C, however, would seem to have caused further oxidation of tellurium from the +4 to the +6 valence state, although  $\text{TeO}_3$  cannot be distinguished from a tellurate [8,15]. Chemical-shift effects in general, but most notably for cesium, were again compatible with a mixed uranate [8].

Representative XPS spectra covering the 210-260 eV binding-energy range, recorded from the four CEX-1 fuels, are compared in Figure 10. Rubidium and cesium both have secondary photoelectron peaks in this region, which provide much of the emission intensity seen for the fragments from the two high-power fuels. Conversely, the two low-power fuels consistently showed distinctive Mo 3d doublets, at binding energies that are characteristic of molybdenum in the +6 valence state, although  $\text{MoO}_3$  cannot be easily distinguished from a molybdate [15]. Further oxidation of molybdenum presumably occurred during the storage exposure, but whether it was initially in a tetravalent or metallic state remains uncertain. Oxidized molybdenum has commonly been found at similar levels on fragments of low/intermediate-power fuels from the CEX-2 experiment as well [9]. The higher power/burnup CANDU fuels that show the greatest segregation of other fission products have not yielded much evidence of molybdenum by XPS regardless of exposure [8,9]. Although there are several potential explanations for such odd behaviour in terms of molybdenum speciation [9], further XPS data on-intact fuels with a wider range of power histories will be needed for a proper assessment.

#### 4. CONCLUSIONS

The XPS results reported here confirm the metallographic observations of pervasive grain-boundary attack during the last CEX-1 storage period in unlimited air; however, the high degrees of oxidation measured (Table 1) must still be largely restricted to very thin films. Detection of fission products at about the levels expected on the basis of the fuel power histories implies an absence of major fuel restructuring. The SEM examinations also revealed mainly subtle changes in the  $\text{UO}_2$  grain structure and suggested only the initial stages of  $\text{U}_3\text{O}_8$  formation over limited areas. These findings are consistent with X-ray diffraction analyses, which have identified  $\text{U}_4\text{O}_9$  and  $\text{U}_3\text{O}_7$  as the predominant alteration phases, with minor amounts of  $\text{U}_3\text{O}_8$  detected in just a few samples [6]. Previous studies of the air oxidation of used CANDU fuel at higher temperatures have demonstrated that massive disruption of the fuel matrix requires considerably greater bulk oxidation.

#### ACKNOWLEDGEMENTS

The authors would like to thank E.L. Bialas, H.G. Delaney and J.D. Chen for providing the diametral  $\gamma$ -ray scans and information on fission-gas release. They are also grateful to J. Freire-Canosa, L.H. Johnson, J. McFarlane, D.W. Shoemith and P. Taylor for constructive criticism of this work. The Canadian Nuclear Fuel Waste Management Program is jointly funded by AECL and Ontario Hydro under the auspices of the CANDU Owners Group.

## REFERENCES

- [1] PATTANTYUS P. and R. BEAUDOIN, "Commercial Applications of Dry Storage Technology", Proc. Internat. Conf. CANDU Fuel, Ed. I.J. HASTINGS, Chalk River, 419-427, 1986.
- [2] WASYWICH K.M. and C.R. FROST, "Current Status of the Canadian Experimental Dry Storage Program for Irradiated Fuel", Proc. Internat. Conf. CANDU Fuel, Ed. I.J. HASTINGS, Chalk River, 367-382, 1986.
- [3] WASYWICH K.M., W.H. HOCKING, D.W. SHOESMITH and P. TAYLOR, "Differences in Oxidation Behaviour of Used CANDU Fuel During Prolonged Storage in Moisture-Saturated Air and Dry Air at 150°C", Nucl. Technol. 104, 309-329, 1993.
- [4] HOCKING W.H., A.F. GERWING, K.M. WASYWICH and C.R. FROST, "X-ray Photoelectron Spectroscopy on Used CANDU Fuel Exposed to Warm Moist-Air Conditions", Proc. Second Internat. Conf. CANDU Fuel, Ed. I.J. HASTINGS, Pembroke, 322-336, 1989.
- [5] WASYWICH K.M., W.H. HOCKING, A.M. DUCLOS, D.R. RANDELL, R. BEHNKE and C.R. FROST, "Oxidation Behaviour of Used CANDU Fuel Stored in Moisture-Saturated Air at 150°C", Proc. Third Internat. Conf. CANDU Fuel, Ed. C.Z. BOCZAR, Pembroke, 9.40-9.53, 1992.
- [6] TAYLOR P., R.J. McEACHERN, S. SUNDER, K.M. WASYWICH, N.H. MILLER and D.D. WOOD, "Recent Findings on the Oxidation of UO<sub>2</sub> Fuel Under Nominally Dry Storage Conditions", Proc. Fourth Internat. Conf. CANDU Fuel (this volume).
- [7] GERWING A.F., F.E. DOERN and W.H. HOCKING, "X-ray Photoelectron Spectroscopy on Radioactive Materials Using a McPherson ESCA-36 Equipped with an SSL Position-Sensitive Detector", Surf. Interface Anal. 14, 559-566, 1989.
- [8] HOCKING W.H., A.M. DUCLOS and L.H. JOHNSON, "Study of Fission-Product Segregation in Used CANDU Fuel by X-ray Photoelectron Spectroscopy (XPS) II", J. Nucl. Mater. 209, 1-26, 1994.
- [9] HOCKING W.H., A.M. DUCLOS, A.F. GERWING and K.M. WASYWICH, "Investigation of the Grain-Boundary Chemistry in Used CANDU Fuel by X-ray Photoelectron Spectroscopy (XPS)", Proc. IAEA Technical Committee Meeting on Recent Developments on Post-Irradiation Examination Techniques for Water-Reactor Fuel, Cadarache, IAEA TECH-DOC (in press).
- [10] HOCKING W.H., R.A. VERRALL, P.G. LUCUTA and HJ. MATZKE, "Depth-Profiling Studies of Ion-Implanted Cesium and Rubidium in SIMFUEL and Uranium Dioxide", Radiat. Effects Defects Solids, 125, 299-321, 1993.

- [11] BEHNKE R., L.C. BROWN and A.K. MCILWAIN, "Performance of the WNRE Shielded SEM", Proc. Second Internat. Conf. CANDU Fuel, Ed. I.J. HASTINGS, Pembroke, 282-291, 1989.
- [12] McINTYRE N.S., S. SUNDER, D.W. SHOESMITH and F.W. STANCHELL, "Chemical Information from XPS — Applications to the Analysis of Electrode Surfaces", J. Vac. Sci. Technol. 18, 714-721, 1981.
- [13] SMITH D.K., B.E. SCHEETZ, C.A.F. ANDERSON and K.L. SMITH, "Phase Relations in the Uranium-Oxygen-Water System and its Significance on the Stability of Nuclear Waste Forms", Uranium, 1, 79-110, 1982.
- [14] THOMAS L.E., C.E. BEYER and L.A. CHARLOT, "Microstructural Analysis of LWR Spent Fuels at High Burnup", J. Nucl. Mater. 188, 80-89, 1992.
- [15] MOULDER J.F., W.F. STICKLE, P.E. SOBOL and K.D. BOMBEN, Ed. J. CHASTAIN, "Handbook of X-ray Photoelectron Spectroscopy", Perkin-Elmer, Eden Prairie, 1992.

TABLE 1. XPS MEASUREMENTS OF INTERNAL OXIDATION IN USED CANDU FUEL

Sample <sup>a</sup>	Location <sup>b</sup>	%U <sup>6+</sup>	$\Delta(\%U^{6+})^c$	U <sup>6+</sup> /U <sup>4+</sup>	SEM Observations <sup>d</sup>
<b>BFO6605C/14, CANLUB, Burnup = 213 MW-h/kg U, Peak (Average) Power = 39 (32) kW/m</b>					
2-I	+75	71	68-74	2.4	Mainly IGF with light ST. Some grain-edge separation and modest SC.
2-O	+75	71	68-74	2.4	Mainly IGF with light ST. Modest SC over entire surface.
8-I	-50	89	85-91	8.1	Weathered TGF suggests in-reactor crack. Moderate SC over entire surface.
8-O	-15	79	77-83	3.8	Mainly IGF but a little TGF. Moderate SC and/or debris in a few areas.
13-I	-170	31	25-37	0.4	Mixture of IGF and TGF with no SC. Reject for XPS analysis.
13-O	-170	57	54-62	1.3	Mainly IGF but a little TGF. Limited grain-edge separation and no SC.
17-I	-280	76	72-80	3.2	Weathered TGF suggests in-reactor crack. Modest SC over entire surface.
17-O	-280	61	57-64	1.6	Mainly IGF with light ST. Some grain-edge separation and modest SC.
<b>BEO4323C/8, CANLUB, Burnup = 186 MW-h/kg U, Peak (Average) Power = 33 (30) kW/m</b>					
2-I	+75	74	71-76	2.8	Mixture of IGF and weathered TGF. Some grain-edge separation but no SC.
2-O	+75	71	69-73	2.4	Mainly IGF with light ST. Some grain-edge separation and modest SC.
8-I	-15	79	77-81	3.8	IGF with light ST. Moderate to heavy SC and/or debris over entire surface.
8-O	-15	59	56-61	1.4	Mixture of cut surface, IGF and TGF. Reject for XPS analysis.
13-I	-160	68	66-70	2.1	Mainly IGF but a little TGF. Some grain-edge separation and modest SC.
13-O	-160	75	73-77	3.0	Mainly IGF. Some grain-edge separation and modest SC.
16-I	-280	57	55-59	1.3	Mainly IGF but a little TGF. Modest to heavy SC and/or debris over limited area.
16-O	-280	59	56-61	1.4	Mainly IGF with light ST. Moderate coverage of SC over most of surface.

continued.....

TABLE 1. XPS MEASUREMENTS OF INTERNAL OXIDATION IN USED CANDU FUEL  
(concluded)

Sample <sup>a</sup>	Location <sup>b</sup>	%U <sup>6+</sup>	$\Delta(\%U^{6+})^c$	U <sup>6+</sup> /U <sup>4+</sup>	SEM Observations <sup>d</sup>
<b>P11171W/7, CANLUB, Burnup = 204 MW·h/kg U, Peak (Average) Power = 50 (46) kW/m</b>					
2-I	+75	70	68-72	2.3	Mainly IGF with some FGB. Moderate SC over entire surface.
2-O	+75	72	68-76	2.6	Weathered TGF suggests in-reactor crack. Modest SC over most of surface.
8-I	-15	72	68-76	2.6	Weathered TGF suggests in-reactor crack. Modest SC over entire surface.
8-O	-15	99	96-100	99	Mainly IGF with light ST. Light SC over most of surface.
13-I	-125	63	59-67	1.7	Mainly IGF with FGB. Modest SC over most of surface.
13-O	-125	74	70-80	2.8	Mainly IGF with some ST. Some grain-edge separation and light SC.
17-I	-280	39	35-44	0.6	IGF with FG bubbles but some TGF. Very little SC.
17-O	-280	55	52-58	1.2	Mainly IGF with a few FGB. Very little or no SC.
<b>P26244C/7, non-CANLUB, Burnup = 222 MW·h/kg U, Peak (Average) Power = 48 (44) kW/m</b>					
2-I	+75	75	72-77	3.0	Mainly IGF but a little TGF. Heavy SC and/or debris over limited area.
2-O	+75	60	56-64	1.5	Mainly IGF with some tiny FGB. Light to moderate SC over most of surface.
8-I	-25	65	60-70	1.6	Mainly IGF with FGB but a little TGF. Little or no SC.
8-O	-25	92	89-94	11	Mainly IGF with distinct ST. Some grain-edge separation but little SC.
13-I	-125	68	63-73	2.1	Mainly IGF with distinct ST. Some grain-edge separation and SC.
13-O	-125	48	44-52	0.9	Mainly IGF with some tiny FGB. Modest SC and/or debris over entire surface.
17-I	-280	74	68-76	2.8	Mainly IGF with some ST. Some grain-edge separation and modest SC.
17-O	-280	66	62-71	1.9	Mainly IGF with some tiny FGB. Modest SC and/or debris over entire surface.

<sup>a</sup> Segment number and nominal radial position: I = near fuel axis and O = toward fuel periphery.

<sup>b</sup> Approximate distance above (+) or below (-) the sheath defect in millimeters.

<sup>c</sup> Probable error range for the %U<sup>6+</sup> values as discussed in the text.

<sup>d</sup> Abbreviations used are: IGF = intergranular fracture, TGF = transgranular fracture, ST = surface texture, FGB = fission-gas bubbles and SC = secondary crystallization.

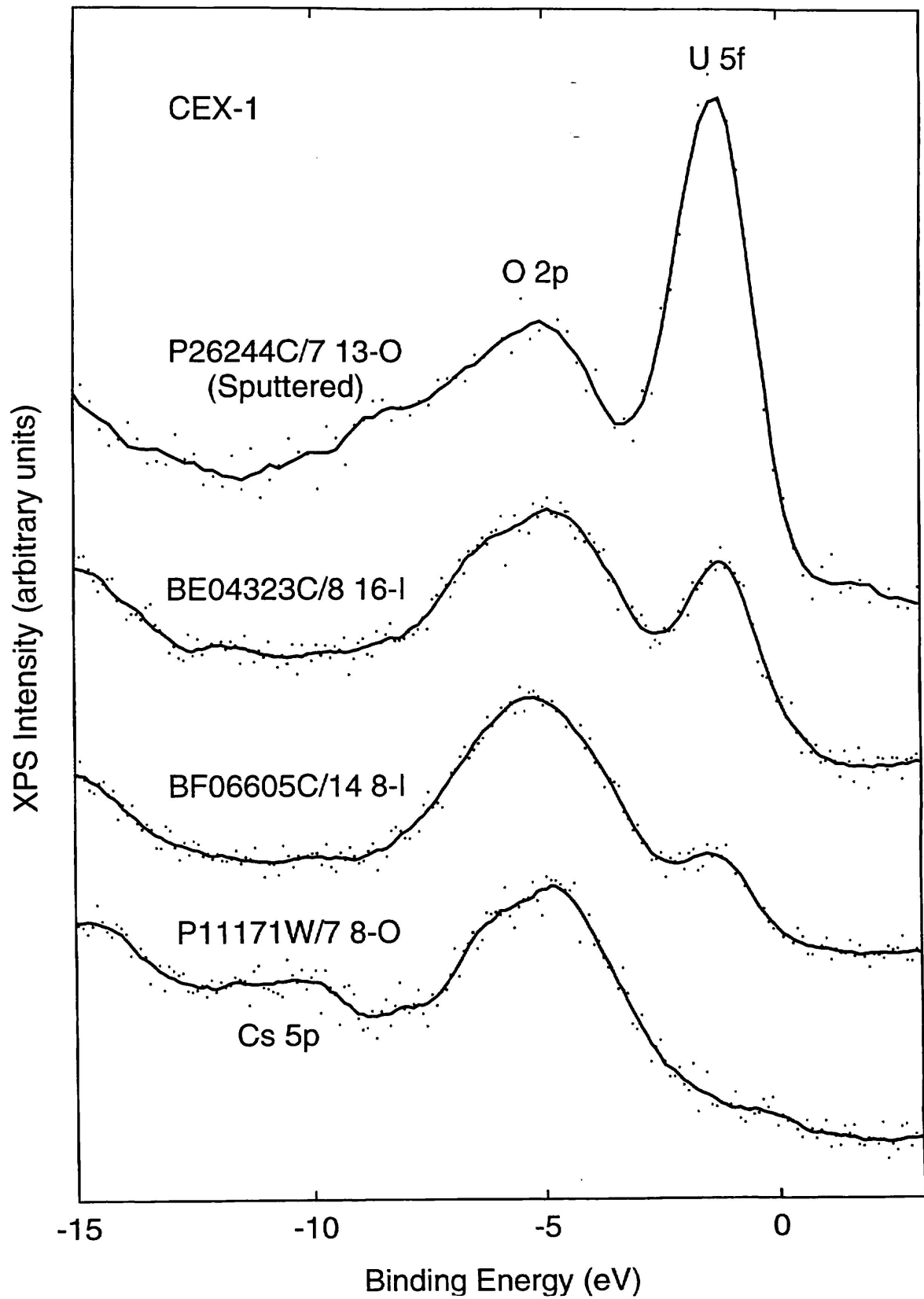


FIGURE 1. CHANGES IN THE XPS VALENCE BAND REFLECT THE URANIUM OXIDATION STATE (UO<sub>2</sub> TOP).



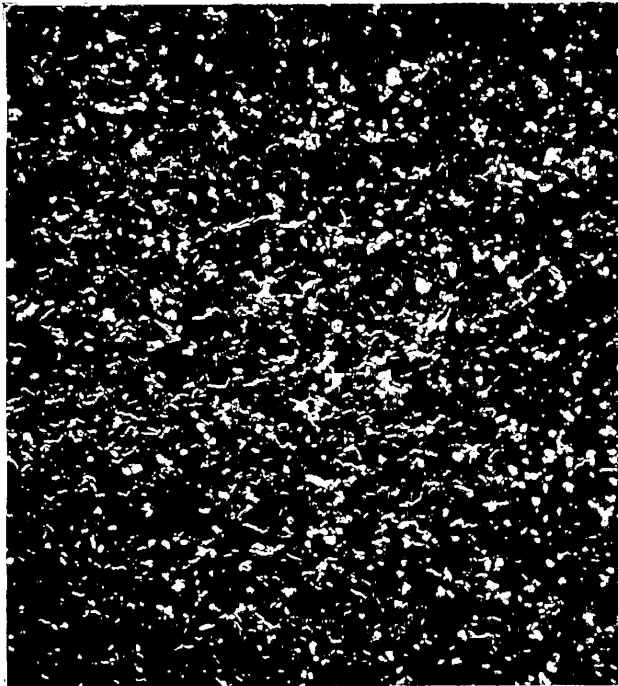
a

1.2 mm



b

12 μm



c

120 μm



d

6 μm

FIGURE 2. SECONDARY ELECTRON IMAGES OF BF06605C/14 FUEL FRAGMENTS 2-I (a, b) AND 17-I (c, d).

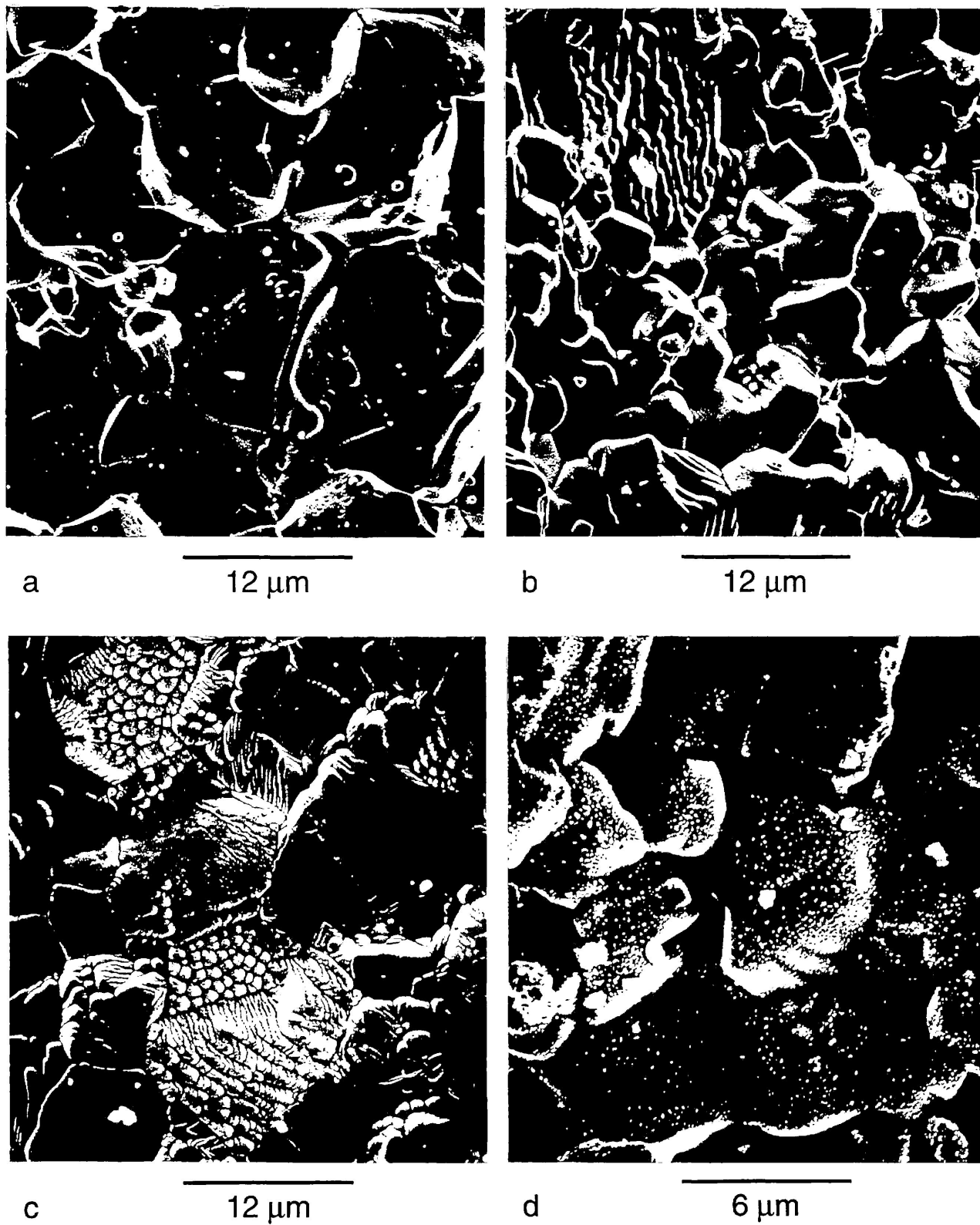


FIGURE 3. SECONDARY ELECTRON IMAGES OF P26244C/7 FUEL FRAGMENTS 8-I (a), 8-O (b), 13-I (c) AND 17-I (d).

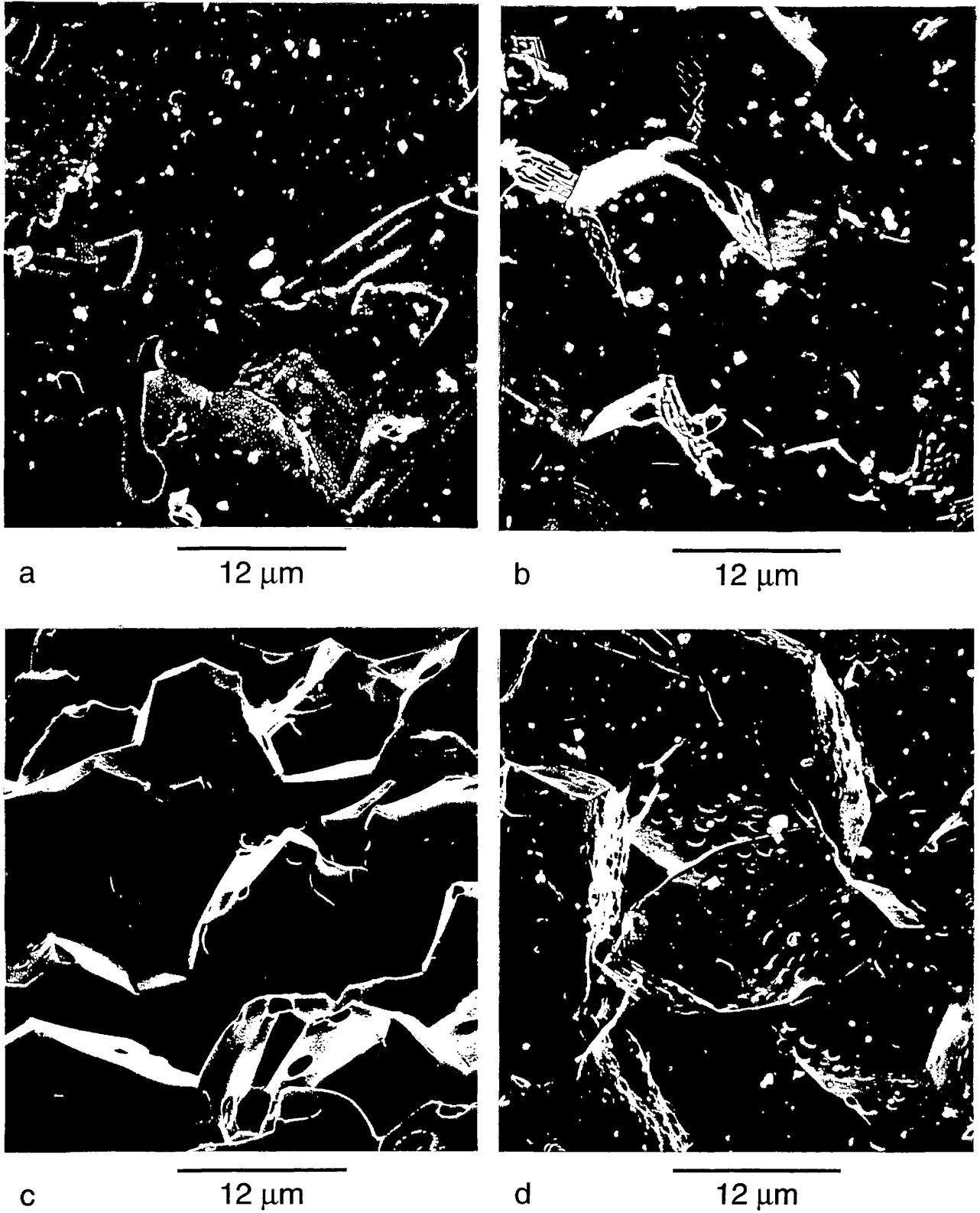
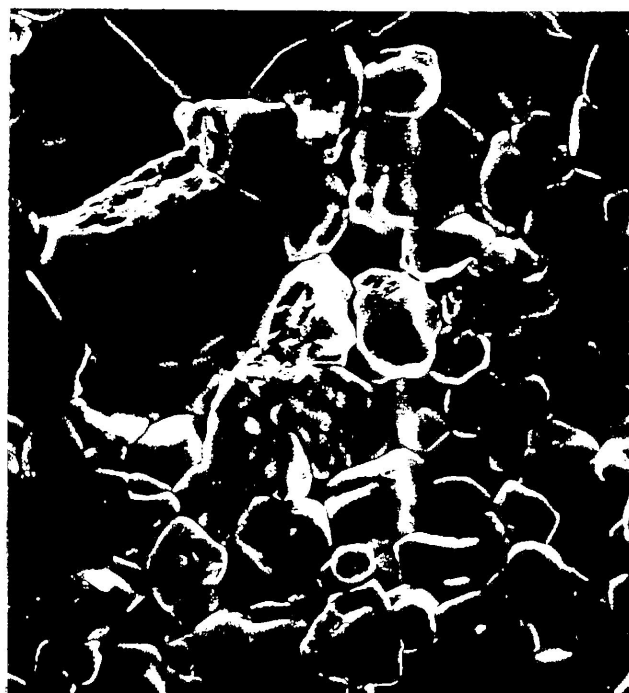


FIGURE 4. SECONDARY ELECTRON IMAGES OF P11171W/7 FUEL FRAGMENTS 2-O (a), 13-O (b), 8-I (c) AND 17-I (d).



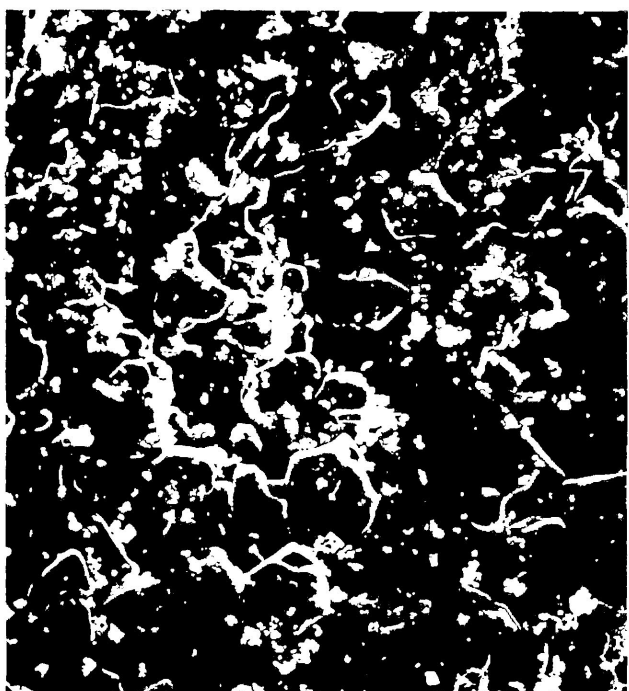
a

12  $\mu$ m



b

6  $\mu$ m



c

12  $\mu$ m



d

12  $\mu$ m

FIGURE 5. SECONDARY ELECTRON IMAGES OF BE04323C/8 FUEL FRAGMENTS 2-I (a), 13-I (b) AND 8-I (c,d).

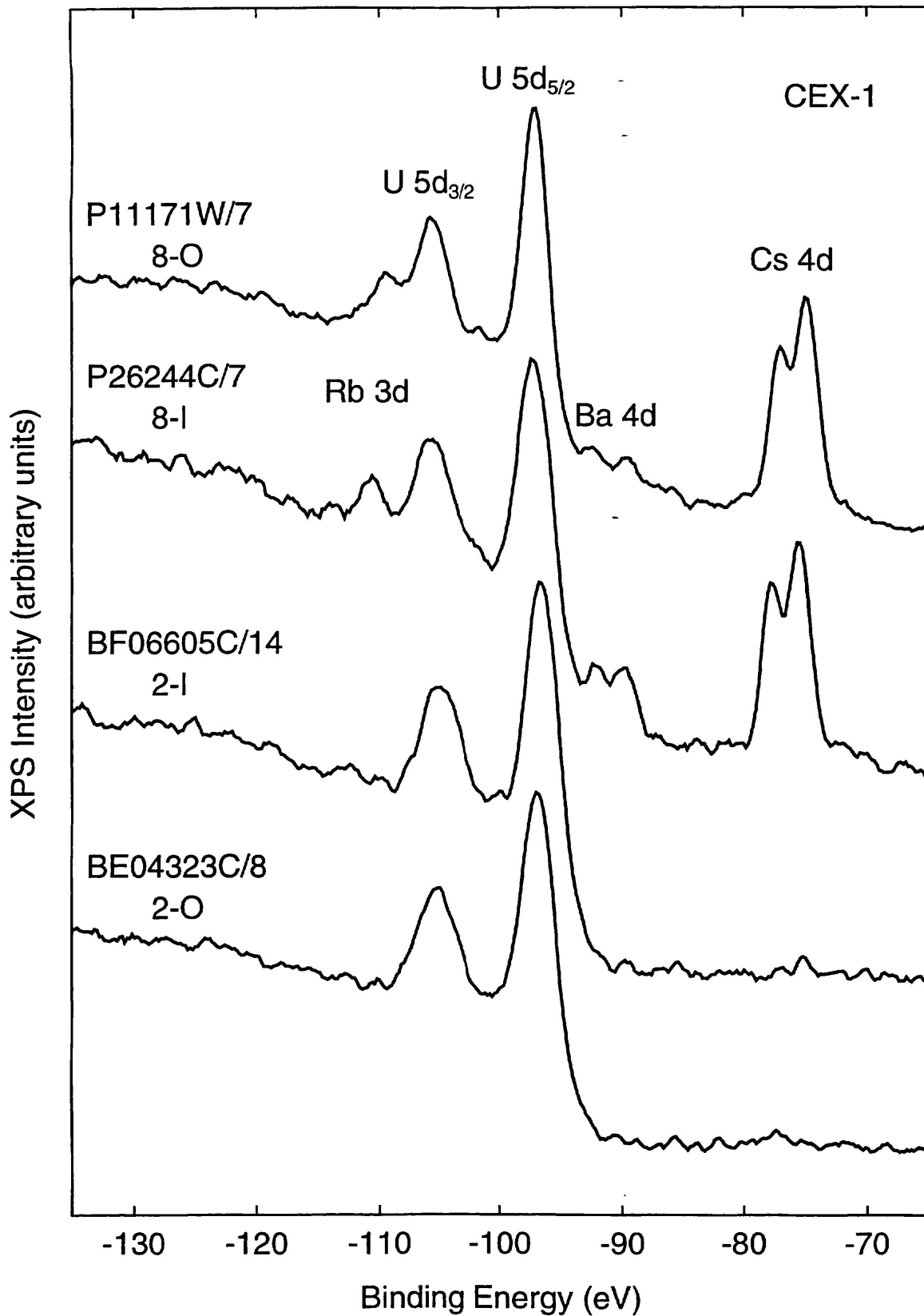


FIGURE 6. TYPICAL XPS SPECTRA ILLUSTRATING FISSION-PRODUCT SEGREGATION ON CEX-1 FUEL FRAGMENTS.

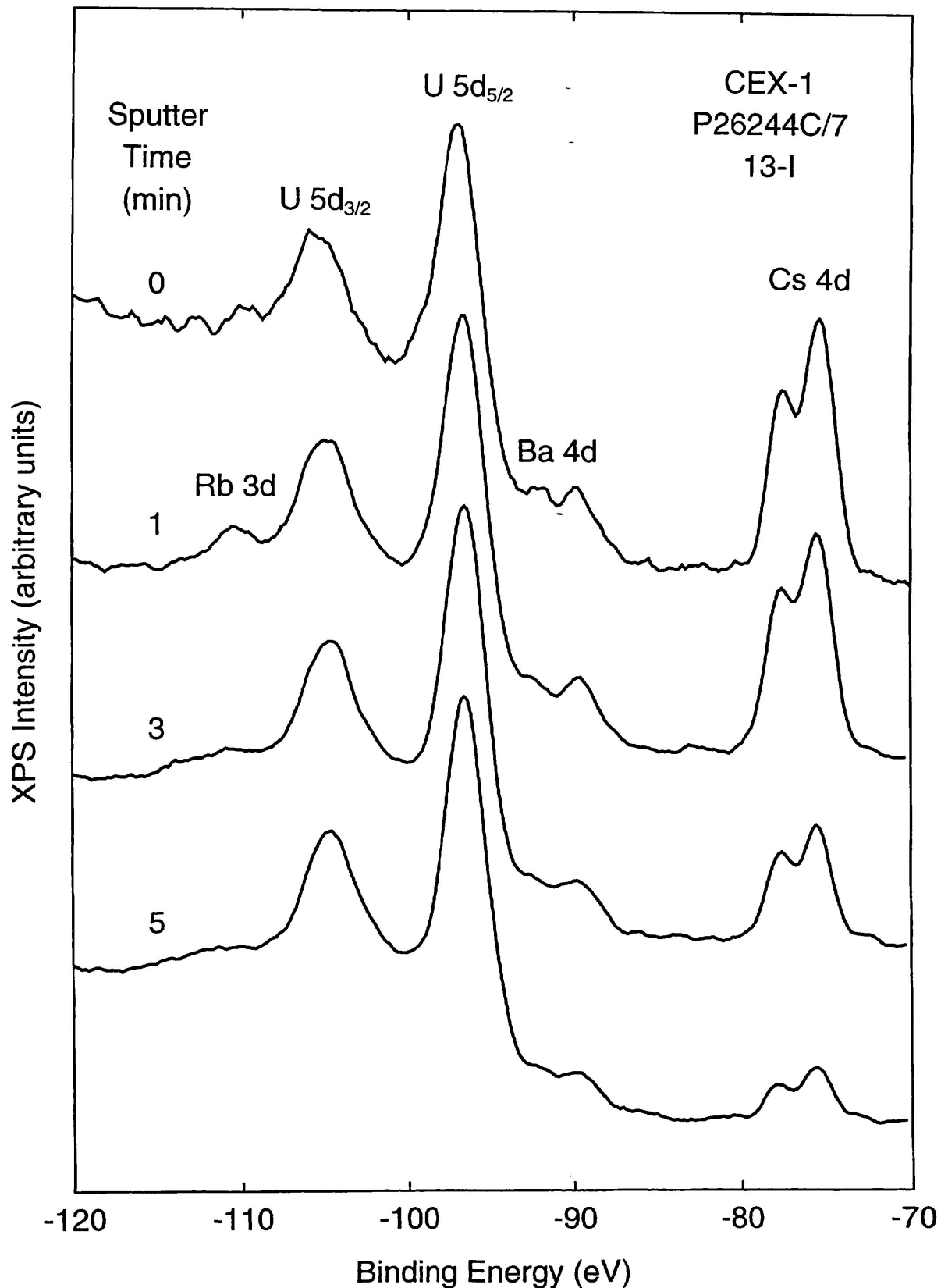


FIGURE 7. SEQUENCE OF XPS SPECTRA AS A FUNCTION OF ARGON-ION SPUTTERING FOR ONE FUEL FRAGMENT.

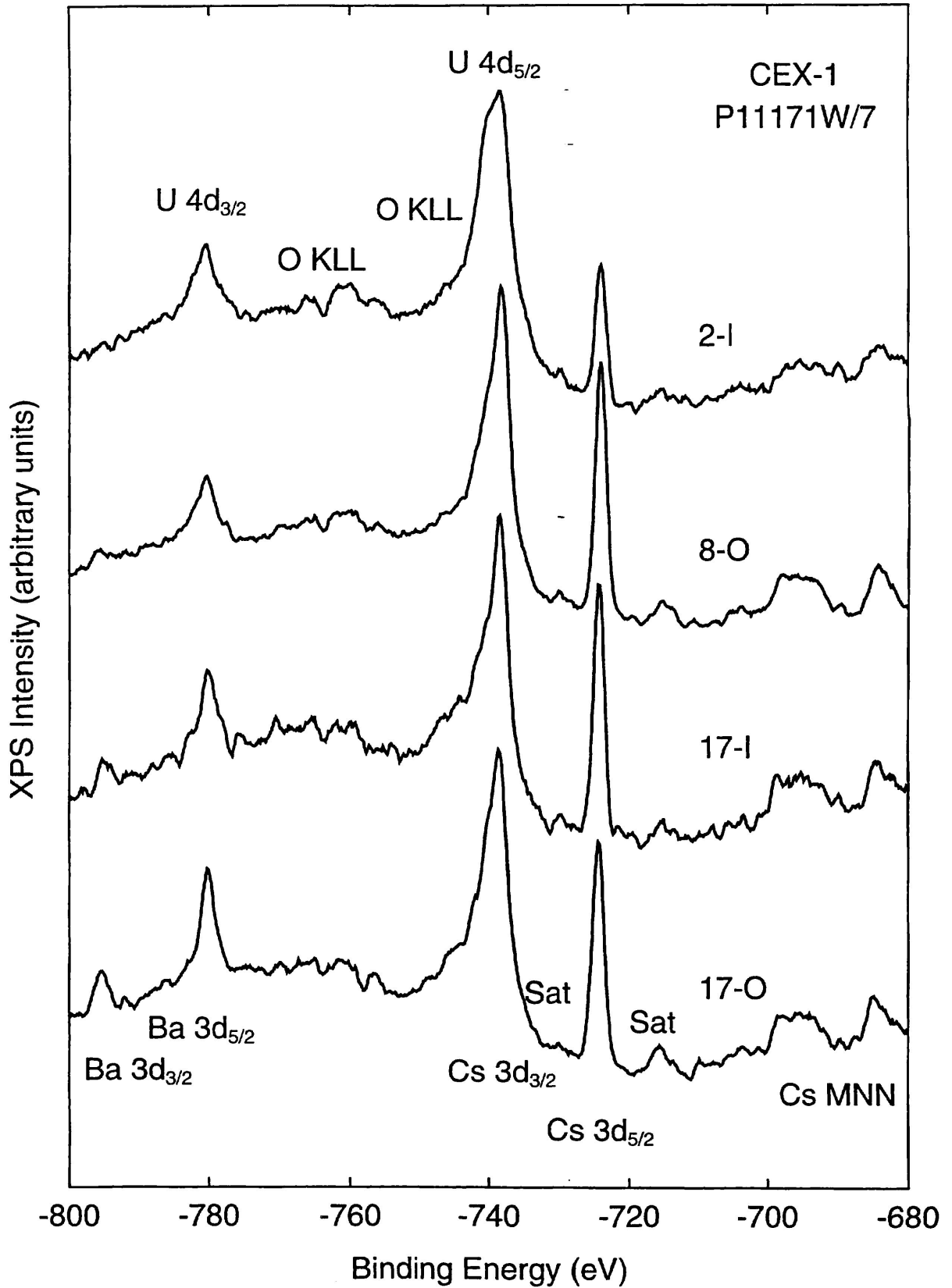


FIGURE 8. SERIES OF XPS SPECTRA SHOWING VARIABILITY IN CESIUM AND BARIUM SEGREGATION.

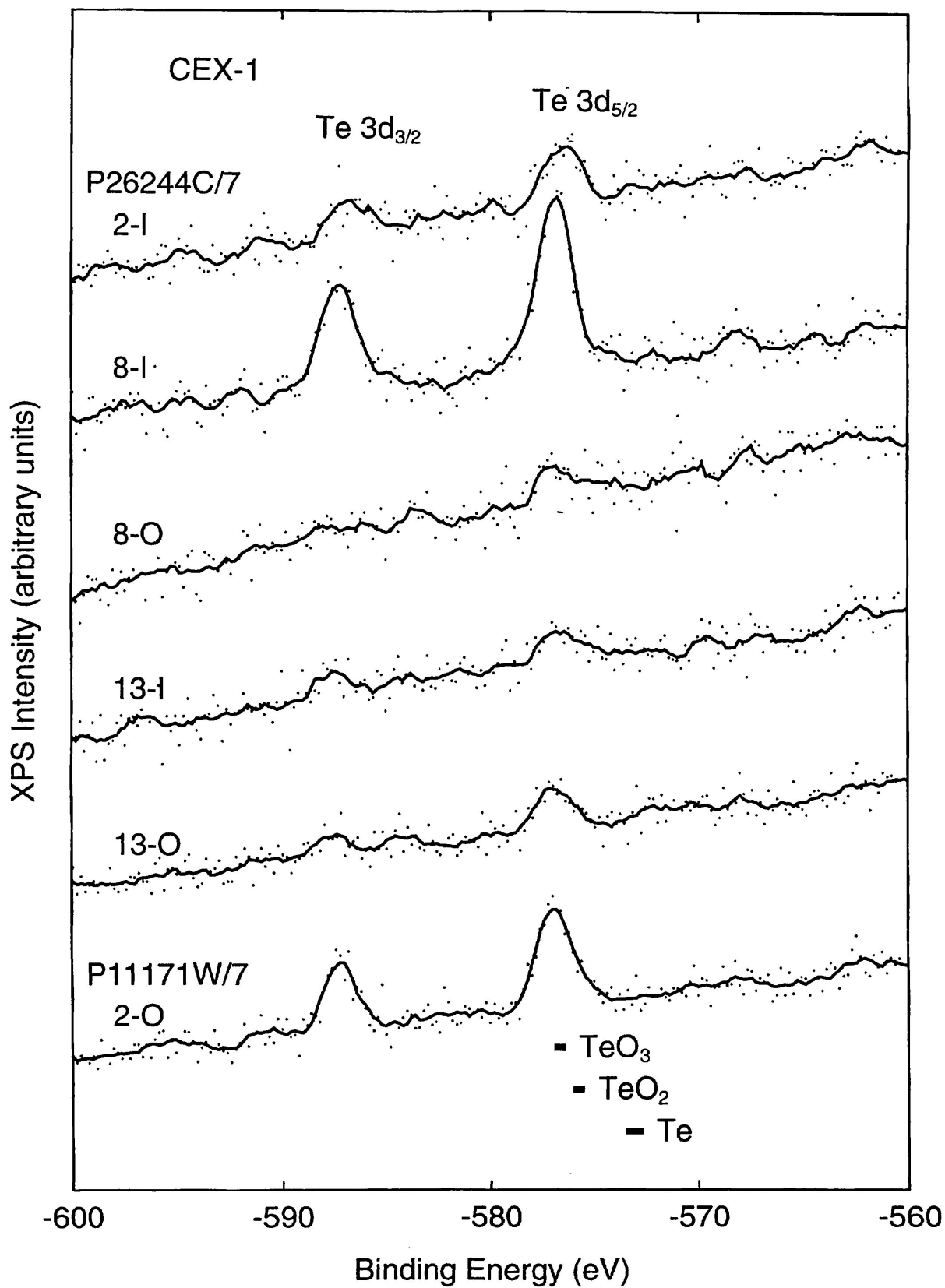


FIGURE 9. SERIES OF XPS SPECTRA SHOWING VARIABILITY IN TELLURIUM SEGREGATION.

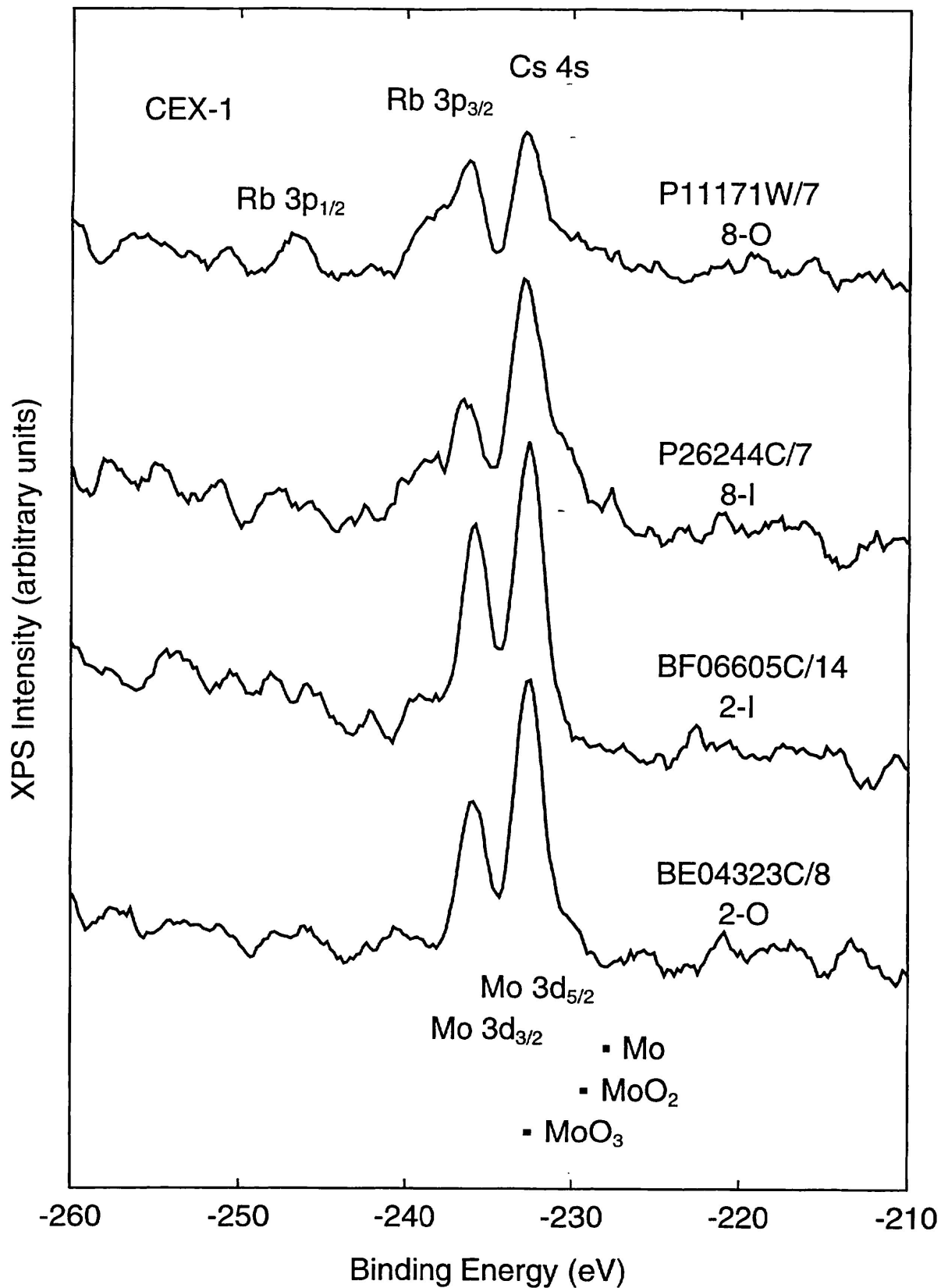


FIGURE 10. TYPICAL XPS SPECTRA ILLUSTRATING PECULIAR MOLYBDENUM SEGREGATION.